Beamformer design for Full-Duplex Amplify-and-Forward millimeter wave relays

Roberto López-Valcarce
atlanTTic Research Center – University of Vigo, Spain
valcarce@gts.uvigo.es

Nuria González-Prelcic
University of Texas at Austin
ngprelcic@utexas.edu

***Abstract*—We consider the design of Amplify & Forward Full-Duplex (FD) relay-assisted communication systems. The FD mode has potential for significant improvements in spectral efficiency, but it suffers from large self-interference (SI) levels. Beamforming-based SI mitigation is attractive for millimeter wave (mmWave) systems due to the large number of degrees of freedom available with large antenna arrays. We first develop an all-digital beamformer design by imposing a zero-forcing constraint on SI, performing quasi-optimally in terms of spectral efficiency. The design is then modified to fit the hardware-related constraints usually found when operating at mmWave, so that the beamformers can be implemented in the analog domain by using phase shifters, with an acceptable performance loss.**

***Index Terms*—Full-duplex, amplify-and-forward relay, millimeter wave communications, analog beamforming.**

I. Introduction

In wireless networks, improved reliability and coverage extension can be achieved by using relays [1]. In particular, Amplify-and-Forward (A&F) relays constitute a low-complexity and highly flexible technology [2]. The Full-Duplex (FD) mode, in which the relay simultaneously receives and transmits on the same frequency channel, has attracted attention due to its potential to improve spectral efficiency with respect the traditional Half-Duplex (HD) mode [3], [4]. However, as in any FD system, it becomes necessary to mitigate the high-power self-interference (SI) leaking from the relay transmitter to its receiver, which is challenging. Since it is critical to avoid saturation of the receiver RF front-end and ADC, SI mitigation typically combines antenna design, analog-domain, and digital-domain cancellation; such techniques have been demonstrated for microwave-band single-antenna FD systems [5]. Analog domain cancellation methods scale poorly with the number of antennas, making their extension to multiple-input multiple-output (MIMO) systems challenging. Nevertheless, MIMO opens the door to *spatial* SI suppression [6]–[9] at the price of lower data rates, because some of the available spatial degrees of freedom (DoF) are sacrificed.

On the other hand, millimeter wave (mmWave) systems incorporate substantially larger antenna arrays [10], [11], providing more DoF and making spatial SI suppression more attractive. The potential of mmWave communications for improving the performance of next-generation networks is widely recognized [11], [12], and the application of FD at mmWave frequencies is gathering interest [13]–[17]. An important feature in mmWave MIMO is the use of hybrid architectures [11], [21], which allow to use fewer power-hungry RF chains than antennas by cascading baseband digital and RF analog beamforming stages. The latter is implemented with phase shifters, imposing a constant-amplitude (CA) constraint on the entries of the analog beamforming matrix: spatial SI suppression methods in FD mmWave systems must take such CA constraints into account. This is not straightforward, and only a few recent works have started to consider this problem. In [17]–[19] a network of two FD mmWave nodes with bidirectional communication was considered, an all-digital design was first derived, and then projected onto the set of feasible hybrid beamformers. However, as discussed in [18], this final projection step is problematic in general. In [20] a mmWave setting is considered, in which a base station communicates with several single-antenna users through a MIMO FD A&F relay, but only results for very low SI levels were reported.

We consider a mmWave two-hop A&F relaying network in which the source and destination nodes communicate through the FD MIMO relay. As in [17], we focus on single-stream transmission with a single RF chain per front-end. Inspired by the approach from [17] for the two-node bidirectional network, we first develop an all-digital design which yields quasi-optimal performance. In this single-stream scenario, and similarly to [18], the final projection approach to obtain the analog beamformers incurs a very significant loss, so we appropriately modify the all-digital design to overcome this issue. The resulting analog design is computationally simple and significantly reduces the aforementioned loss.

II. Problem setting

Fig. 1 shows a mmWave network consisting of a source node S, an FD relay node R and a destination node D. Node S transmits a data stream to R using an array of $N_{\rm S}$ antennas. The relay R is equipped with receive and transmit antenna arrays of sizes $N_{\rm R}$ and $N_{\rm T}$, respectively, whereas node D uses a receive array of size $N_{\rm D}$. We assume that there is no direct link from S to D. The channels are assumed frequency-flat, and the matrices for the S $\rightarrow$ R and R $\rightarrow$ D links are respectively denoted as $\boldsymbol{H}_{\rm SR}$ (size $N_{\rm R}\times N_{\rm S}$) and $\boldsymbol{H}_{\rm RD}$ (size $N_{\rm D}\times N_{\rm T}$). The

Work supported in part by the Agencia Estatal de Investigación (Spain), in part by the European Regional Development Fund (ERDF) through projects WINTER (TEC2016-76409-C2-2-R) and MYRADA (TEC2016-75103-C2-2-R), and in part by the Xunta de Galicia (Agrupación Estratéxica Consolidada de Galicia accreditation 2016-2019).

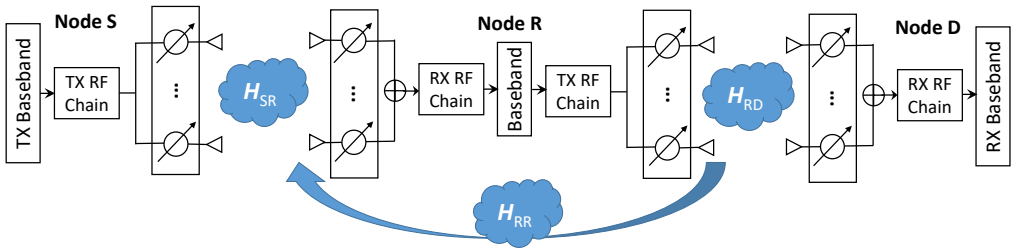

Fig. 1. FD relay network with analog TX/RX beamforming.

SI channel, with size $N_{\rm R} \times N_{\rm T}$, is denoted by $\boldsymbol{H}_{\rm RR}$. Since the proposed designs are model-independent, the discussion on specific channel models is postponed to Sec. V, where numerical results will be presented.

Let $\boldsymbol{f}$ denote the complex-valued $N_{\rm S} \times 1$ beamforming vector applied by node S before transmission; and let $\boldsymbol{v}$ denote the $N_{\rm D} \times 1$ combiner applied by node D. Similarly, let $\boldsymbol{w}$ (size $N_{\rm R} \times 1$) and $\boldsymbol{b}$ (size $N_{\rm T}$) be the corresponding beamformers ar R. With analog-domain beamforming using phase shifters, the entries of $\boldsymbol{f}$, $\boldsymbol{w}$, $\boldsymbol{b}$ and $\boldsymbol{v}$ have constant magnitude. The average transmit power per symbol at S is $\rho_{\rm S}$, and the noise vectors $\boldsymbol{n}_{\rm R}$, $\boldsymbol{n}_{\rm D}$ at the receive side of R and D are zero-mean Gaussian with covariance $\sigma_{\rm R}^2 \boldsymbol{I}_{N_{\rm R}}$ and $\sigma_{\rm D}^2 \boldsymbol{I}_{N_{\rm D}}$ respectively.

The signal received at R can be written as

$$y_{\rm R} = \boldsymbol{w}^H(\sqrt{\rho_{\rm S}}\boldsymbol{H}_{\rm SR}\boldsymbol{f}s + \sqrt{\rho_{\rm SI}}\boldsymbol{H}_{\rm RR}\boldsymbol{b}z + \boldsymbol{n}_{\rm R}), \quad (1)$$

where s is the symbol sent from S, and z is the SI affecting R. Both s and z have unit variance, with $\rho_{\rm SI}$ quantifying SI strength. Due to relay processing delay and hardware imperfections, z is a delayed and distorted version of the signal transmitted by R. In practice the relay will be equipped with additional passive and/or active SI cancellation stages, so that z is to be understood as residual SI left over by those stages.

The relay operates in A&F mode, so that its received signal y_R is amplified with power gain g and retransmitted. In this way, the signal received at D is given by

$$y_{\rm D} = \boldsymbol{v}^H(\sqrt{g}\boldsymbol{H}_{\rm RD}\boldsymbol{b}y_{\rm R} + \boldsymbol{n}_{\rm D}). \quad (2)$$

It can be assumed w.l.o.g. that $\|\boldsymbol{f}\| = \|\boldsymbol{w}\| = \|\boldsymbol{b}\| = \|\boldsymbol{v}\| = 1$. Then, treating SI as noise and assuming Gaussian codebooks, the achievable rate of this network is given by

$$\mathcal{R} = \log_2\left(1 + \frac{g\rho_{\rm S}|\boldsymbol{v}^H\boldsymbol{H}_{\rm RD}\boldsymbol{b}|^2|\boldsymbol{w}^H\boldsymbol{H}_{\rm SR}\boldsymbol{f}|^2}{\sigma_{\rm D}^2 + g\sigma_{\rm R}^2|\boldsymbol{v}^H\boldsymbol{H}_{\rm RD}\boldsymbol{b}|^2 + g\rho_{\rm SI}|\boldsymbol{v}^H\boldsymbol{H}_{\rm RD}\boldsymbol{b}|^2|\boldsymbol{w}^H\boldsymbol{H}_{\rm RR}\boldsymbol{b}|^2}\right) \quad (3)$$

A. Design problem

The goal is to maximize $\mathcal{R}$ in (3) w.r.t. $\boldsymbol{f}$, $\boldsymbol{w}$, $\boldsymbol{b}$, $\boldsymbol{v}$ and g subject to the following constraints:

1) **Unit-norm:** All four vectors $\boldsymbol{f}$, $\boldsymbol{w}$, $\boldsymbol{b}$, $\boldsymbol{v}$ have unit norm.
2) **Constant-amplitude (CA):** Each of the entries of vectors $\boldsymbol{f}$, $\boldsymbol{w}$, $\boldsymbol{b}$, $\boldsymbol{v}$ has constant magnitude.
3) **Relay power:** Let $\rho_{\rm R} > 0$ denote the maximum available transmit power at R. Then $g\mathbb{E}\{|y_{\rm R}|^2\} \le \rho_{\rm R}$, i.e.,

$$g\left(\rho_{\rm S}|\boldsymbol{w}^H\boldsymbol{H}_{\rm SR}\boldsymbol{f}|^2 + \rho_{\rm SI}|\boldsymbol{w}^H\boldsymbol{H}_{\rm RR}\boldsymbol{b}|^2 + \sigma_{\rm R}^2\right) \le \rho_{\rm R}. \quad (4)$$

It is useful to introduce the following variables:

$$\epsilon_{\rm R} \triangleq \frac{\rho_{\rm S}}{\sigma_{\rm R}^2}, \quad \epsilon_{\rm D} \triangleq \frac{\rho_{\rm R}}{\sigma_{\rm D}^2}, \quad \epsilon_{\rm SI} \triangleq \frac{\rho_{\rm SI}}{\rho_{\rm S}}, \quad q \triangleq \frac{\sigma_{\rm R}^2}{\sigma_{\rm D}^2}g. \quad (5)$$

Note that $\epsilon_{\rm R}$, $\epsilon_{\rm D}$, and $\epsilon_{\rm SI}$ denote the SNR at R and D, and the self-interference to useful signal ratio at R, respectively, when the corresponding channels have unit gain. Additionally, let us introduce the equivalent power gains

$$h_{\rm SR}^2(\boldsymbol{w},\boldsymbol{f}) = |\boldsymbol{w}^H\boldsymbol{H}_{\rm SR}\boldsymbol{f}|^2, \quad (6)$$
$$h_{\rm RD}^2(\boldsymbol{v},\boldsymbol{b}) = |\boldsymbol{v}^H\boldsymbol{H}_{\rm RD}\boldsymbol{b}|^2, \quad (7)$$
$$h_{\rm RR}^2(\boldsymbol{w},\boldsymbol{b}) = |\boldsymbol{w}^H\boldsymbol{H}_{\rm RR}\boldsymbol{b}|^2. \quad (8)$$

With these, the rate $\mathcal{R}$ in (3) can be rewritten as

$$\mathcal{R} = \log_2\left(1 + \frac{q\epsilon_{\rm R}h_{\rm SR}^2(\boldsymbol{w},\boldsymbol{f})h_{\rm RD}^2(\boldsymbol{v},\boldsymbol{b})}{1 + q\left(1 + \epsilon_{\rm R}\epsilon_{\rm SI}h_{\rm RR}^2(\boldsymbol{w},\boldsymbol{b})\right)h_{\rm RD}^2(\boldsymbol{v},\boldsymbol{b})}\right), \quad (9)$$

whereas the relay power constraint (4) becomes

$$q\left(\epsilon_{\rm R}h_{\rm SR}^2(\boldsymbol{w},\boldsymbol{f}) + \epsilon_{\rm R}\epsilon_{\rm SI}h_{\rm RR}^2(\boldsymbol{w},\boldsymbol{b}) + 1\right) \le \epsilon_{\rm D}. \quad (10)$$

B. Performance upper bound

In order to benchmark the performance of the different designs, it is useful to have an upper bound to (9). It can be obtained assuming no SI ($\epsilon_{\rm SI} = 0$) and dropping the CA constraints. Then, using the fact that for any $a \ge 0$

$$f(x) = \frac{x}{a + x} \quad \text{monotonically increases in } x \ge 0, \quad (11)$$

it follows that $\mathcal{R} \le \mathcal{R}^\star$, with

$$\mathcal{R}^\star \triangleq \log_2\left(1 + \frac{\epsilon_{\rm R}\epsilon_{\rm D}\sigma_1^2(\boldsymbol{H}_{\rm SR})\sigma_1^2(\boldsymbol{H}_{\rm RD})}{1 + \epsilon_{\rm R}\sigma_1^2(\boldsymbol{H}_{\rm SR}) + \epsilon_{\rm D}\sigma_1^2(\boldsymbol{H}_{\rm RD})}\right), \quad (12)$$

with $\sigma_1(\boldsymbol{A})$ denoting the largest singular value of $\boldsymbol{A}$.

III. All-digital design

Due to the coupling between $\boldsymbol{w}$ and $\boldsymbol{b}$ in the term $h_{\rm RR}^2(\boldsymbol{w},\boldsymbol{b})$, maximizing (9) is not a convex problem even if the CA constraints are dropped. Inspired by the fact that, for a two-node bidirectional network with FD nodes, imposing Zero-Forcing (ZF) constraints on the SI yields close-to-optimal

performance [17], we will follow a similar approach. The resulting problem is:

$$\max \quad \log_2\left(1+\frac{q\epsilon_{\rm R}h^2_{\rm SR}(\boldsymbol{w},\boldsymbol{f})h^2_{\rm RD}(\boldsymbol{v},\boldsymbol{b})}{1+qh^2_{\rm RD}(\boldsymbol{v},\boldsymbol{b})}\right) \tag{13}$$

$$\text{s. to} \quad q\geq 0, \quad \|\boldsymbol{f}\|=\|\boldsymbol{w}\|=\|\boldsymbol{b}\|=\|\boldsymbol{v}\|=1, \tag{14}$$

$$q\left(\epsilon_{\rm R}h^2_{\rm SR}(\boldsymbol{w},\boldsymbol{f})+1\right)\leq \epsilon_{\rm D}, \tag{15}$$

$$h^2_{\rm RR}(\boldsymbol{w},\boldsymbol{b})=0. \tag{16}$$

Note that by virtue of the ZF constraint (16), the SI is cancelled in the *analog domain,* specifically at the input of the receive RF chain in Fig. 1. Using fact (11), it is readily seen that (13) is maximized w.r.t. q when (15) is satisfied with equality, i.e., when the relay transmits at full power. In this way, Problem (13)-(16) becomes:

$$\max \quad \log_2\left(1+\frac{\epsilon_{\rm R}\epsilon_{\rm D}h^2_{\rm SR}(\boldsymbol{w},\boldsymbol{f})h^2_{\rm RD}(\boldsymbol{v},\boldsymbol{b})}{1+\epsilon_{\rm R}h^2_{\rm SR}(\boldsymbol{w},\boldsymbol{f})+\epsilon_{\rm D}h^2_{\rm RD}(\boldsymbol{v},\boldsymbol{b})}\right) \tag{17}$$

$$\text{s. to} \quad \|\boldsymbol{f}\|=\|\boldsymbol{w}\|=\|\boldsymbol{b}\|=\|\boldsymbol{v}\|=1, \quad h^2_{\rm RR}(\boldsymbol{w},\boldsymbol{b})=0. \tag{18}$$

By virtue of fact (11), $\boldsymbol{f}$ and $\boldsymbol{v}$ are obtained as the unit-norm vectors maximizing $h^2_{\rm SR}(\boldsymbol{w},\boldsymbol{f})$ and $h^2_{\rm RD}(\boldsymbol{v},\boldsymbol{b})$, respectively, for fixed $\boldsymbol{w}$ and $\boldsymbol{b}$:

$$\boldsymbol{f}=\frac{\boldsymbol{H}^H_{\rm SR}\boldsymbol{w}}{\|\boldsymbol{H}^H_{\rm SR}\boldsymbol{w}\|}, \qquad \boldsymbol{v}=\frac{\boldsymbol{H}_{\rm RD}\boldsymbol{b}}{\|\boldsymbol{H}_{\rm RD}\boldsymbol{b}\|}. \tag{19}$$

Substituting (19) in (17), the problem becomes

$$\max_{\boldsymbol{w},\boldsymbol{b}} \ \log_2\left(1+\frac{\epsilon_{\rm R}\epsilon_{\rm D}\|\boldsymbol{H}^H_{\rm SR}\boldsymbol{w}\|^2\|\boldsymbol{H}_{\rm RD}\boldsymbol{b}\|^2}{1+\epsilon_{\rm R}\|\boldsymbol{H}^H_{\rm SR}\boldsymbol{w}\|^2+\epsilon_{\rm D}\|\boldsymbol{H}_{\rm RD}\boldsymbol{b}\|^2}\right) \tag{20}$$

$$\text{s. to} \quad \|\boldsymbol{w}\|=\|\boldsymbol{b}\|=1, \qquad \boldsymbol{w}^H\boldsymbol{H}_{\rm RR}\boldsymbol{b}=0. \tag{21}$$

This problem does not admit a closed-form solution for $\boldsymbol{w}$ or $\boldsymbol{b}$, because of the coupling between variables due to the ZF constraint in (21). Analogously to [17], we propose to tackle this problem using a cyclic maximization approach:

1) In the first step, hold the TX beamforming vector $\boldsymbol{b}$ fixed to its value from the previous iteration, and then maximize (20) w.r.t. $\boldsymbol{w}$ subject to the unit norm and ZF constraints:

$$\max_{\boldsymbol{w}} \|\boldsymbol{H}^H_{\rm SR}\boldsymbol{w}\|^2 \quad \text{s.to} \quad \|\boldsymbol{w}\|=1, \ \boldsymbol{w}^H\boldsymbol{H}_{\rm RR}\boldsymbol{b}=0. \tag{22}$$

2) Hold fixed the RX beamforming vector $\boldsymbol{w}$ obtained in this way, and then maximize w.r.t. $\boldsymbol{b}$:

$$\max_{\boldsymbol{b}} \|\boldsymbol{H}_{\rm RD}\boldsymbol{b}\|^2 \quad \text{s.to} \quad \|\boldsymbol{b}\|=1, \ \boldsymbol{w}^H\boldsymbol{H}_{\rm RR}\boldsymbol{b}=0. \tag{23}$$

These two steps are then iterated until convergence. Note that at each iteration the objective function (20) is increased, or at least not decreased; therefore, the sequence of objective values along the iterations must converge since it is bounded above.

It remains to solve (22)-(23). These two subproblems have the same generic form: given $\boldsymbol{G}\in\mathbb{C}^{M\times N}$ and $\boldsymbol{c}\in\mathbb{C}^N$,

$$\max_{\boldsymbol{x}} \quad \|\boldsymbol{G}\boldsymbol{x}\|^2 \quad \text{s. to} \quad \|\boldsymbol{x}\|^2=1, \quad \boldsymbol{x}^H\boldsymbol{c}=0. \tag{24}$$

In Problem (22), we take $\boldsymbol{x}=\boldsymbol{w}$, $\boldsymbol{c}=\boldsymbol{H}_{\rm RR}\boldsymbol{b}$ and $\boldsymbol{G}=\boldsymbol{H}^H_{\rm SR}$, whereas in Problem (23) we take $\boldsymbol{x}=\boldsymbol{b}$, $\boldsymbol{c}=\boldsymbol{H}^H_{\rm RR}\boldsymbol{w}$ and $\boldsymbol{G}=\boldsymbol{H}_{\rm RD}$. The general solution of (24) is given in the next result, whose proof is skipped for lack of space.

Lemma 1. *Let $\boldsymbol{P}_\perp$ be the projection matrix onto the subspace orthogonal to $\boldsymbol{c}$:*

$$\boldsymbol{P}_\perp=\boldsymbol{I}_N-\frac{\boldsymbol{c}\boldsymbol{c}^H}{\|\boldsymbol{c}\|^2}. \tag{25}$$

Then the solution $\boldsymbol{x}_\star$ to Problem (24) *is the principal unit-norm eigenvector of $\boldsymbol{P}_\perp\boldsymbol{G}^H\boldsymbol{G}$, yielding $\|\boldsymbol{G}\boldsymbol{x}_\star\|^2=\lambda_1(\boldsymbol{P}_\perp\boldsymbol{G}^H\boldsymbol{G})$, where $\lambda_1(\boldsymbol{A})$ is the largest eigenvalue of $\boldsymbol{A}$.*

Hence, the all-digital design proceeds by solving (22)-(23) iteratively with the aid of Lemma 1. Upon convergence, $\boldsymbol{w}$, $\boldsymbol{b}$ are obtained, and then $\boldsymbol{f}$, $\boldsymbol{v}$ are computed via (19), and finally, the relay gain is then set to achieve full power transmission.

Recall, however, that this all-digital design has neglected the CA constraints on the beamforming vectors $\boldsymbol{f}$, $\boldsymbol{w}$, $\boldsymbol{b}$, $\boldsymbol{v}$. A straightforward approach is to project the all-digital solutions onto the set of unit-norm CA vectors (by dividing each entry by its corresponding magnitude, and then scaling the resulting vector to unit norm). This *final projection* method, however, entails a significant performance loss as shown in Sec. V, mainly because the resulting vectors $\boldsymbol{w}$, $\boldsymbol{b}$ need not satisfy the ZF constraint, resulting in large SI levels.

IV. Analog design

Instead of projecting the all-digital solutions, the proposed analog design seeks vectors that satisfy the ZF and CA constraints simultaneously and at every iteration of the cyclic maximization procedure (22)-(23). To this end, let us define the set of N-dimensional unit-norm CA vectors as

$$\mathcal{V}^N=\left\{\boldsymbol{v}\in\mathbb{C}^N \,\middle|\, v_i=\frac{1}{\sqrt{N}}e^{j\theta_i}, \, i=1,\ldots,N\right\}. \tag{26}$$

Then we introduce explicitly the CA constraint $\boldsymbol{w}\in\mathcal{V}^{N_{\rm R}}$ in subproblem (22) and $\boldsymbol{b}\in\mathcal{V}^{N_{\rm T}}$ in subproblem (23). With this, the modified subproblems can be generically written as

$$\max_{\boldsymbol{x}} \quad \|\boldsymbol{G}\boldsymbol{x}\|^2 \quad \text{s. to} \quad \boldsymbol{x}\in\mathcal{V}^N, \quad \boldsymbol{x}^H\boldsymbol{c}=0. \tag{27}$$

In contrast with (24), (27) does not have a closed-form solution. We propose to find a feasible point $\boldsymbol{x}$ for (27), i.e., simultaneously satisfying $\boldsymbol{x}\in\mathcal{V}^N$ and $\boldsymbol{x}^H\boldsymbol{c}=0$, by using the method of alternating projections [22], which iteratively project the current estimate onto $\mathcal{V}^N$ and the subspace orthogonal to $\boldsymbol{c}$. To avoid convergence to a small value of the objective function, these alternating projections are initialized at a point corresponding to a large objective value (cf. the solution provided by Lemma 1), with the hope that successive projections will not wander too far away from it. These *inner* iterations (alternating projections) should be run for each of the two basic subproblems which are part of each *outer* iteration of the cyclic maximization procedure.

Once the relay beamformers $\boldsymbol{w}$, $\boldsymbol{b}$ are obtained, the beamforming vectors at S and D are computed by

$$\max_{\boldsymbol{f}} |\boldsymbol{w}^H\boldsymbol{H}_{\rm SR}\boldsymbol{f}|^2 \quad \text{s. to} \quad \boldsymbol{f}\in\mathcal{V}^{N_{\rm S}}, \tag{28}$$

$$\max_{\boldsymbol{v}} |\boldsymbol{v}^H\boldsymbol{H}_{\rm RD}\boldsymbol{b}|^2 \quad \text{s. to} \quad \boldsymbol{v}\in\mathcal{V}^{N_{\rm D}}, \tag{29}$$

which can be solved in closed form; specifically, the solutions are given by the projections of $\boldsymbol{H}^H_{\rm SR}\boldsymbol{w}$ and $\boldsymbol{H}_{\rm RD}\boldsymbol{b}$ onto $\mathcal{V}^{N_{\rm S}}$

and $\mathcal{V}^{N_\mathrm{D}}$, respectively. Finally, the relay gain is set for full power transmission. Algorithm 1 summarizes the design.

Algorithm 1 Analog beamformer design

function ALTPR($\boldsymbol{G}$, $\boldsymbol{c}$, N)
  $\boldsymbol{x} \leftarrow$ principal 1-norm eigenvector of $\left(\boldsymbol{G} - \frac{\boldsymbol{G}\boldsymbol{c}\boldsymbol{c}^H}{\boldsymbol{c}^H\boldsymbol{c}}\right)^H \boldsymbol{G}$
  for $k \leftarrow 1, N_\mathrm{inner}$ **do**
    $\widetilde{\boldsymbol{x}} \leftarrow \boldsymbol{x} - \frac{\boldsymbol{c}^H\boldsymbol{x}}{\boldsymbol{c}^H\boldsymbol{c}}\boldsymbol{c}$
    for $i \leftarrow 1, N$ **do** $x_i \leftarrow \frac{1}{\sqrt{N}} \frac{\widetilde{x}_i}{|\widetilde{x}_i|}$
    end for
  end for
  return $\boldsymbol{x}$
end function

Input: $\boldsymbol{H}_\mathrm{SR}$, $\boldsymbol{H}_\mathrm{RD}$, $\boldsymbol{H}_\mathrm{RR}$, ρ_R, ρ_S, ρ_SI, σ_R^2
Initialize $\boldsymbol{w}$, $\boldsymbol{b}$
for $t \leftarrow 1, N_\mathrm{outer}$ **do**
  $\boldsymbol{w} \leftarrow$ ALTPR$(\boldsymbol{H}_\mathrm{SR}^H, \boldsymbol{H}_\mathrm{RR}\boldsymbol{b}, N_\mathrm{R})$
  $\boldsymbol{b} \leftarrow$ ALTPR$(\boldsymbol{H}_\mathrm{RD}, \boldsymbol{H}_\mathrm{RR}^H\boldsymbol{w}, N_\mathrm{T})$
end for
$\widetilde{\boldsymbol{f}} \leftarrow \boldsymbol{H}_\mathrm{SR}^H\boldsymbol{w}$
for $i \leftarrow 1, N_\mathrm{S}$ **do** $f_i \leftarrow \frac{1}{\sqrt{N_\mathrm{S}}} \frac{\widetilde{f}_i}{|\widetilde{f}_i|}$
end for
$\widetilde{\boldsymbol{v}} \leftarrow \boldsymbol{H}_\mathrm{RD}\boldsymbol{b}$
for $i \leftarrow 1, N_\mathrm{D}$ **do** $v_i \leftarrow \frac{1}{\sqrt{N_\mathrm{D}}} \frac{\widetilde{v}_i}{|\widetilde{v}_i|}$
end for
$g \leftarrow \frac{\rho_\mathrm{R}}{\sigma_\mathrm{R}^2 + \rho_\mathrm{S}|\boldsymbol{w}^H\boldsymbol{H}_\mathrm{SR}\boldsymbol{f}|^2 + \rho_\mathrm{SI}|\boldsymbol{w}^H\boldsymbol{H}_\mathrm{RR}\boldsymbol{b}|^2}$

V. Numerical results

We present simulation results for the setting of Fig. 1 with the S, Rand D nodes having their antennas arranged in uniform linear arrays (ULAs) with half-wavelength ($\lambda/2$) separation between adjacent elements. The distance and angle between the TX and RX ULAs of R are $d = 2\lambda$ and $\omega = \frac{\pi}{2}$ respectively, see [18, Fig. 2]. The number of antennas is set to $N_\mathrm{S} = N_\mathrm{R} = N_\mathrm{T} = N_\mathrm{D} = 16$. For the S→R and R→D channels, we consider the narrowband clustered model from [21], with N_cl scattering clusters and N_ray paths per cluster. The channel matrices $\boldsymbol{H}_\mathrm{SR}$, $\boldsymbol{H}_\mathrm{RD}$ are then given by

$$\boldsymbol{H}_\mathrm{SR/RD} = \sum_{k=1}^{N_\mathrm{cl}} \sum_{\ell=1}^{N_\mathrm{ray}} \beta_{k,\ell} \boldsymbol{a}_\mathrm{r}(\phi_{k,\ell}^j) \boldsymbol{a}_\mathrm{t}^*(\theta_{k,\ell}^i), \tag{30}$$

where $\beta_{k,\ell}$ is the complex gain of the ℓ^th ray in the k^th cluster, and $\boldsymbol{a}_\mathrm{t}(\theta_{k,\ell}^i)$ and $\boldsymbol{a}_\mathrm{r}(\phi_{k,\ell}^j)$ are the antenna array steering and response vectors at the transmitter and receiver, respectively, evaluated at the corresponding azimuth angles of departure from transmitter at node i, $\theta_{k,\ell}^i$, or arrival at node j, $\phi_{k,\ell}^j$. We assumed $N_\mathrm{cl} = 4$ clusters with $N_\mathrm{ray} = 10$ paths per cluster. Departure/arrival angles are random, with mean cluster angle uniformly distributed in $[0, 360°]$ and angular spreads of $15°$. All the path gains have the same variance and are independently drawn from a circular complex Gaussian distribution.

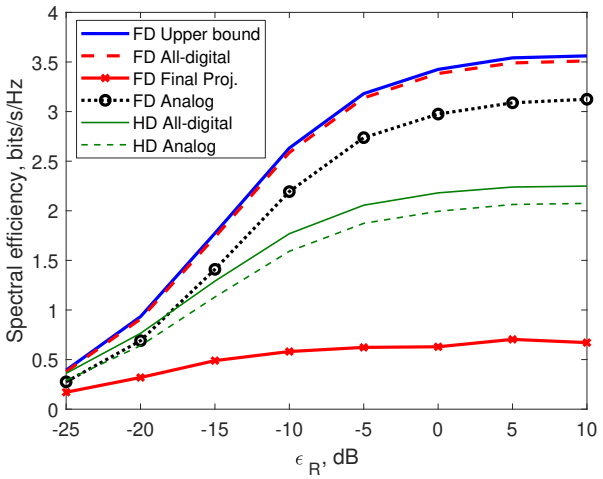

Fig. 2. Performance results. $\epsilon_\mathrm{D} = -10$ dB, $\epsilon_\mathrm{SI} = 30$ dB.

The TX and RX arrays of node R are are assumed close to each other, and thus a line-of-sight near-field model is adopted for the SI channel $\boldsymbol{H}_\mathrm{RR}$ [13], [14], [17], [18]: letting d_{pq} be the distance between the p-th antenna of the TX array and the q-th antenna of the RX array, then

$$[\boldsymbol{H}_\mathrm{RR}]_{pq} = \frac{1}{d_{pq}} e^{-j2\pi \frac{d_{pq}}{\lambda}}. \tag{31}$$

All channel matrices are normalized so that their respective Frobenius norms equal the product of the corresponding column and row dimensions.

The spectral efficiency was computed for the different designs by averaging over 200 Monte Carlo runs. For comparison we also show the achievable rate for the Half-Duplex setting, in which the available bandwidth is split in half between the S→R and R→D links, yielding half the noise powers as in the FD case. With full-power relay transmission, this rate is

$$\mathcal{R}_\mathrm{HD} = \frac{1}{2}\log_2\left(1 + \frac{2\epsilon_\mathrm{R}\epsilon_\mathrm{D} h_\mathrm{SR}^2(\boldsymbol{w},\boldsymbol{f}) h_\mathrm{RD}^2(\boldsymbol{v},\boldsymbol{b})}{\frac{1}{2} + \epsilon_\mathrm{R} h_\mathrm{SR}^2(\boldsymbol{w},\boldsymbol{f}) + \epsilon_\mathrm{D} h_\mathrm{RD}^2(\boldsymbol{v},\boldsymbol{b})}\right). \tag{32}$$

Assuming all-digital beamformers, (32) is maximized when $h_\mathrm{SR}^2(\boldsymbol{w},\boldsymbol{f}) = \sigma_1^2(\boldsymbol{H}_\mathrm{SR})$ and $h_\mathrm{RD}^2(\boldsymbol{v},\boldsymbol{b}) = \sigma_1^2(\boldsymbol{H}_\mathrm{RD})$. For an HD analog design with CA beamformers, we cyclically maximize $h_\mathrm{SR}^2(\boldsymbol{w},\boldsymbol{f})$ w.r.t. $\boldsymbol{w}$ and $\boldsymbol{f}$, and similarly for $h_\mathrm{RD}^2(\boldsymbol{v},\boldsymbol{b})$.

For the all-digital FD and analog HD design, 20 cyclic-maximization iterations were run. For the analog FD design in Algorithm 1 we set $N_\mathrm{outer} = N_\mathrm{inner} = 20$. The beamformers were randomly initialized in all cases.

Fig. 2 shows the spectral efficiency obtained by different designs in terms of the SNR at the relay ϵ_R. The SNR at D is $\epsilon_\mathrm{D} = -10$ dB and the SI-to-signal ratio is $\epsilon_\mathrm{SI} = 30$ dB. Although the FD all-digital design performs close to the upper bound (12), a large degradation is observed if the corresponding solution is projected onto the set of CA vectors, and in fact the performance is worse than that of HD designs. The proposed FD analog design provides a CA solution at a

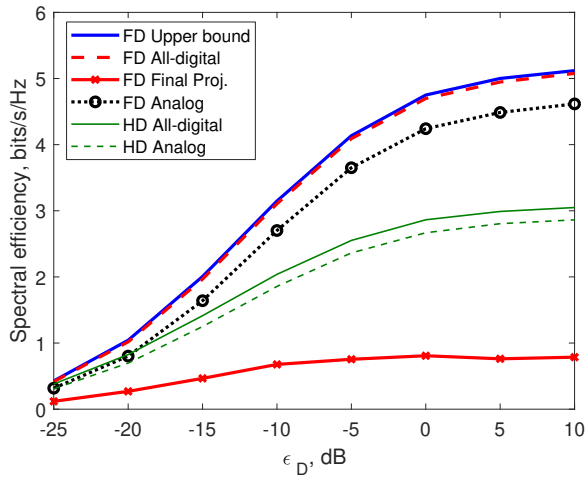

Fig. 3. Performance results. $\epsilon_{\rm R} = -5$ dB, $\epsilon_{\rm SI} = 30$ dB.

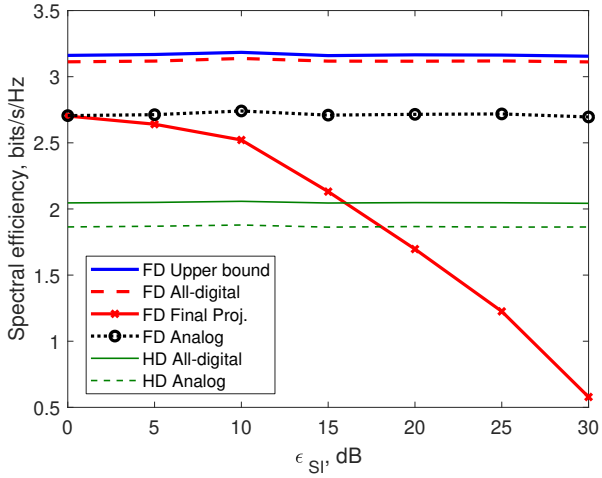

Fig. 4. Performance results. $\epsilon_{\rm R} = -5$ dB, $\epsilon_{\rm D} = -10$ dB.

moderate loss with respect to the all-digital one. In Fig. 3 we fixed $\epsilon_{\rm R} = -5$ dB and varied $\epsilon_{\rm D}$, with similar conclusions. Note that in either FD or HD modes, the spectral efficiency is limited by the minimum of $\epsilon_{\rm R}$ and $\epsilon_{\rm D}$, and that the ratio of FD to HD efficiencies is in general smaller than 2 (it goes to 2 asymptotically as *both* $\epsilon_{\rm R}, \epsilon_{\rm D} \to \infty$ simultaneously).

Finally, in Fig. 4 we set $\epsilon_{\rm R} = -5$ dB, $\epsilon_{\rm D} = -10$ dB and varied $\epsilon_{\rm SI}$. The HD designs are obviously independent of $\epsilon_{\rm SI}$. This is also the case for the FD all-digital and analog designs which enforce the ZF condition, but not when the all-digital design is projected to obtain a CA solution: in that case, spectral efficiency drops sharply as SI strength increases.

VI. Conclusion

The proposed ZF-based all-digital beamformer design for A&F Full-Duplex mmWave relays performs close to the upper bound by effectively suppressing SI in the analog domain, but simply projecting the corresponding beamformers onto the set of CA vectors violates the ZF constraint on the SI. The large performance loss incurred is overcome by the proposed analog design, which enforces the ZF constraint at all steps. Knowledge of the SNRs is needed only to set the relay gain, but since the optimal strategy is for the relay to transmit at full power, with slowly-varying channels this can be achieved by automatic gain control. The sensitivity of the designs to channel estimation errors will be the subject of future research.

References

[1] D. Soldani and S. Dixit, "Wireless relays for broadband access," *IEEE Commun. Mag.,* vol. 46, no. 3, pp. 58–66, Mar. 2008.

[2] L. Jimenez Rodriguez, N. Tran and T. Le-Ngoc, *Amplify-and-Forward Relaying in Wireless Communications.* Springer, 2015.

[3] A. Sabharwal, P. Schniter, D. Guo, D. Bliss, S. Rangarajan and R. Wichman, "In-band full-duplex wireless: Challenges and opportunities," *IEEE J. Sel. Areas Commun.,* vol. 32, no. 9, pp. 1637–1652, Sep. 2014.

[4] Z. Zhang, K. Long, A. V. Vasilakos and L. Hanzo, "Full-duplex wireless communications: Challenges, solutions, and future research directions," *Proc. IEEE,* vol. 104, no. 7, pp. 1369–1409, Jul. 2016.

[5] M. Heino *et al.,* "Recent advances in antenna design and interference cancellation algorithms for in-band full-duplex relays," *IEEE Commun. Mag.,* vol. 53, no. 5, pp. 91–101, May 2015.

[6] T. Riihonen, S. Werner and R. Wichman, "Mitigation of loopback self-interference in full-duplex MIMO relays," *IEEE Trans. Signal Process.,* vol. 59, no. 12, pp. 5983–5993, Dec. 2011.

[7] B. Day, A. Margetts, D. Bliss and P. Schniter, "Full-duplex MIMO relaying: Achievable rates under limited dynamic range," *IEEE J. Sel. Areas Commun.,* vol. 30, no. 8, pp. 1541–1553, Sep. 2012.

[8] S. Huberman and T. Le-Ngoc, "MIMO full-duplex precoding: A joint beamforming and self-interference cancellation structure," *IEEE Trans. Wireless Commun.,* vol. 14, no. 4, pp. 2205–2217, Apr. 2015.

[9] A. Almradi, P. Xiao and K. A. Hamdi, "Hop-by-Hop ZF beamforming for MIMO full-duplex relaying with co-channel interference," *IEEE Trans. Commun.,* vol. 66, no. 12, pp. 6135–6149, Dec. 2018.

[10] Z. Pi and F. Khan, "An introduction to mmwave mobile broadband systems," *IEEE Commun. Mag.,* vol. 49, no. 6, pp. 101-107, Jun. 2011.

[11] R. W. Heath Jr. *et al.,* "An overview of signal processing techniques for millimeter wave MIMO systems," *IEEE J. Sel. Topics Signal Process.,* vol. 10, no. 3, pp. 436–453, Apr. 2016.

[12] S. Rangan, T. S. Rappaport and E. Erkip, "Millimeter-wave cellular wireless networks: Potentials and challenges," *Proc. IEEE,* vol. 102, no. 3, pp. 366–385, Mar. 2014.

[13] Liangbin Li, K. Josiam and R. Taori, "Feasibility study of full-duplex wireless millimeter-wave systems," *Proc. IEEE Int. Conf. Acoust., Speech, Signal Process.,* 2014, pp. 2769–2773.

[14] S. Rajagopal, R. Taori and S. Abu-Surra, "Self-interference mitigation for in-band mmWave wireless backhaul," *Proc. IEEE Consumer Commun. Netw. Conf.,* 2014, pp. 551–556.

[15] A. Demir, T. Haque, E. Bala and P. Cabrol, "Exploring the possibility of Full-Duplex operations in mmWave 5G systems," *Proc. IEEE Wireless Microw. Technol. Conf.,* 2016.

[16] G. Yang and M. Xiao, "Performance analysis of millimeter-wave relaying: Impacts of beamwidth and self-interference," *IEEE Trans. Commun.,* vol. 66, no. 2, pp. 589–600, Feb. 2018.

[17] X. Liu *et al.,*"Beamforming based Full-Duplex for millimeter-wave communication," *Sensors,* 16, 1130, Jul. 2016.

[18] Z. Xiao, P. Xia and X.-G. Xia, "Full-duplex millimeter-wave communication," *IEEE Wireless Commun.,* pp. 136–143, Dec. 2017.

[19] K. Satyanarayana *et al.,* "Hybrid beamforming design for full-duplex mmwave communication," *IEEE Trans. Veh. Technol.,* vol 68, no. 2, pp. 1394–1404, Feb. 2019.

[20] Y. Cai *et al.,* "Robust hybrid transceiver design for millimeter wave full-duplex MIMO relay systems," *IEEE Trans. Wireless Commun.,* vol 18, no. 2, pp. 1199–1215, Feb. 2019.

[21] O. El Ayach, S. Rajagopal, S. Abu-Surra, Z. Pi, R. W. Heath, Jr., "Spatially sparse precoding in mmWave MIMO systems," *IEEE Trans. Wireless Commun.,* vol. 13, no. 3, pp. 1499–1513, Mar. 2014.

[22] R. Escalante and M. Raydan, *Alternating projection methods.* Society for Industrial and Applied Mathematics, vol. 8, 2011.